JOURNAL OF GEOPHYSICAL RESEARCH, VOL. 103, NO. E4, PAGES 8575–8580, APRIL 25, 1998

Electrostatic charging properties of Apollo 17 lunar dust

Mihály Horányi

Laboratory for Atmospheric and Space Physics, University of Colorado, Boulder

Bob Walch

Physics Department, University of Northern Colorado, Greeley

Scott Robertson and David Alexander

Physics Department, University of Colorado, Boulder

Abstract. We report on our experimental studies of the electrostatic charging properties of an Apollo 17 soil sample and two lunar simulants, Minnesota Lunar Simulant (MLS-1) and Johnson Space Center (JSC-1). We have measured their charge after exposing individual grains to a beam of fast electrons with energies in the range of $20 \leq E \leq 90$ eV. Our measurements indicate that the secondary electron emission yield of the Apollo 17 sample is intermediate between MLS-1 and JSC-1, closer to that of MLS-1.

1. Introduction

After a long break following the Apollo missions, the Moon is likely to become again the target of in situ scientific investigations. Perhaps one of the most interesting and controversial science issue from the Apollo era remains the possible electrostatic levitation and transport of lunar dust [*Gold and Williams*, 1973]. This issue is also of great engineering importance in designing and protecting optical devices, for example.

Transient dust clouds suspended above the lunar surface were indicated by the horizon glow observed by the Surveyor spacecrafts [*Rennilson and Criswell*, 1973], by the Lunar Ejecta and Meteorite Experiment (LEAM) deployed during the Apollo 17 mission [*Berg et al.*, 1973], and by the visual observations of the Apollo astronauts [*Zook and McCoy*, 1991]. The available theoretical models cannot fully explain these observations. However, the models suggest that electrostatic charging of the lunar surface due to exposure to the solar wind plasma and UV radiation could result in levitation, transport, and ejection of small grains [*Singer and Walker*, 1962; *Criswell*, 1973; *De and Criswell*, 1977; *Criswell and De*, 1977; *Berg*, 1978].

To conduct laboratory investigations of the surface dust transport on the Moon, we need to find substitute materials that reproduce the electrostatic charging properties of the lunar fines. The chemical and mineralogical composition of lunar dust is well matched by two widely used lunar simulants: Minnesota Lunar Simulant (MLS-1) [*Weiblen et al.*, 1990] and Johnson Space Center (JSC-1) [*McKay et al.*, 1994]. However, their charging properties were not compared to that of the lunar soil. The charge state of grains on the lunar surface is determined by the competition between UV-induced photoelectron production and plasma bombardment. Here we report on our experiments addressing the latter only.

We have constructed an experiment where individual dust grains can be exposed to a thermal plasma background and a flux of fast electrons. We have conducted experiments using glass, copper, graphite, and silicon particles [*Walch et al.*, 1995] and also grains from MLS-1 and JSC-1 lunar substitute materials [*Horányi et al.*, 1995]. Below we report our new set of measurements comparing Apollo 17, MLS-1, and JSC-1 samples. To ensure consistency and to demonstrate reproducibility, we have repeated our earlier MLS-1 and JSC-1 measurements.

2. Apparatus and Theoretical Background

The apparatus (Figure 1) is the same double plasma machine that we used in our earlier experiments [*Walch et al.*, 1995; *Horányi et al.*, 1995]. Fast electrons are created at one end of a cylindrical vacuum chamber (30 cm diameter by 30 cm long) by an emissive tungsten filament biased to a negative potential ($-100 < -U < -10$ V). These electrons impinge on falling dust particles and also ionize the background neutral argon gas.

Dust grains are dropped into the chamber at the top and are collected in a Faraday cup mounted in a diagnostic arm below the chamber. We placed a small per-

Paper number 98JE00486.
0148-0227/98/98JE-00486$09.00

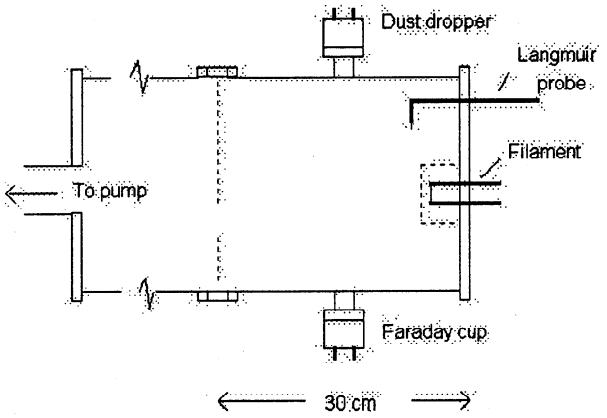

Figure 1. Schematic diagram of the experiment used for dust charge measurements. The dust particles enter the plasma from the dropper at the top and fall through the plasma into the Faraday cup below the chamber.

manent magnet outside the exit hole to prevent electrons and ions from entering the Faraday cup. The Faraday cup is connected to a sensitive electrometer for measuring the charge on the grains. The dropping mechanism, a vibrating plate with a small hole, is adjusted to drop particles infrequently so that the majority of events are due to individual grains. Signals from multiple grains are easily identified by their waveform and are not used.

The filament current is set to 2 mA, which is sufficient to make the charging time for the dust (a 30 μm radius grain takes 50 ms to charge to 30 V) much shorter than the dust transit time through the apparatus (250 ms). The filament is surrounded by a grounded wire mesh so that the potential within the chamber is not distorted by the filament potential. The chamber has a base pressure 4×10^{-7} torr and the experiments were performed with 2×10^{-6} torr of argon. The fast electrons also ionize the background argon gas creating a thermal plasma background. The characteristics of the plasma are measured by a Langmuir probe [*Hershkowitz*, 1989], placed close to the exit hole of the grains. Due to the energy dependence of the electron-neutral ionization cross section [*McDaniel*, 1964] and the changes in the fast electron fluxes entering the apparatus, the plasma conditions change with the bias potential (i.e., the energy of the fast electrons). The measured flux of fast electrons (J_f^0), and the temperature (T_e) and the flux of thermal electrons (J_e^0) as a function of the bias potential are plotted in (Figure 2). We repeated these Langmuir probe measurements before and after the data were taken for each bias potential setting. There were no noticable drifts in the plasma parameters during the data taking period of a sample material. However, they did change between the samples, most likely due to small changes in pressure of the neutral background. In the analysis, we used the corresponding plasma measurements for each of the samples. The error bars in Figure 2 indicate the long-term variability of the plasma parameters.

The ion current is very small and it cannot be determined directly. However, because the ion-neutral collision mean free path is much longer than the size of our device, the argon ions will not remain in thermal equilibrium with the neutral gas. The plasma potential in the center of our device, ϕ_p, will adjust to maintain a balance between the electron and ion currents reaching the walls. Hence the ions will be accelerated toward the walls, arriving there with a mean energy of $e\phi_p/2 \simeq kT_i/2$, where T_i is the ion temperature. The thermal electron (J_e) and ion (J_i) fluxes to the walls (or to a dust grain) are

$$J_e = J_e^o \times \begin{cases} \exp(+e\phi/kT_e) & \phi < 0 \\ 1 + e\phi/kT_e & \phi \geq 0 \end{cases} \tag{1}$$

$$J_i = J_i^o \times \begin{cases} 1 - e\phi/kT_i & \phi < 0 \\ \exp(-e\phi/kT_i) & \phi \geq 0 \end{cases}$$

where e is the magnitude of the charge of an electron and ϕ is the wall (grain) potential relative to the plasma potential [*Whipple*, 1981; *Goertz*, 1989].

The balance between the electron and ion thermal currents to the walls can be written as

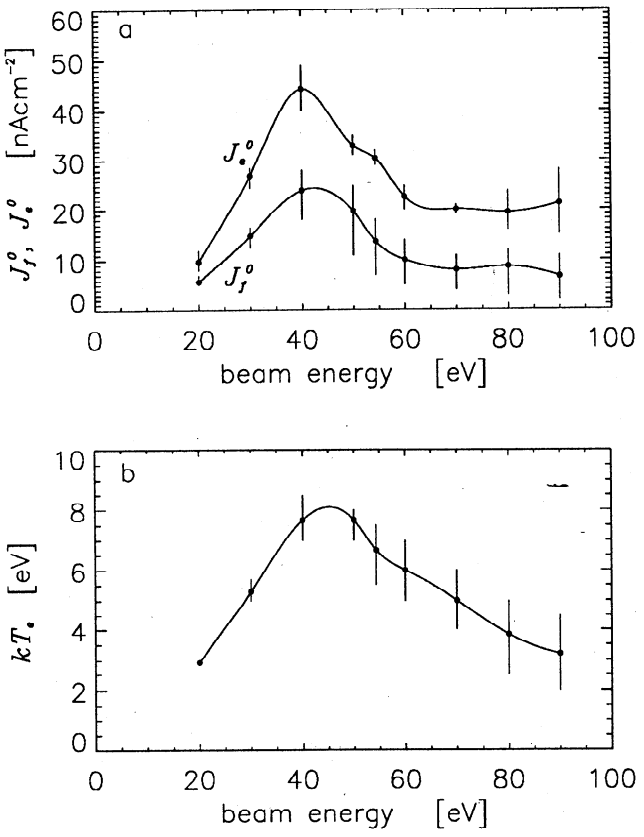

Figure 2. Plasma parameters J_f^0, J_e^0 (a) and kT_e (b) as functions of the fast electron beam energy, determined from Langmuir probe traces. The ion temperature is assumed to be $kT_i = 4kT_e$.

$$\exp\left(-\frac{T_i}{T_e}\right) = 2\left(\frac{m_e T_i}{m_i T_i}\right)^{1/2}, \quad (2)$$

resulting in $kT_i \simeq 4kT_e$, where m_e and m_i are the electron and ion masses, respectively.

The flux of fast electrons, with energy $E = eU$, minus the secondary electron flux induced by them is [*Draine and Salpeter*, 1979; *Propenko and Laframboise*, 1980; *Hershkowitz*, 1989]

$$J_f = J_f^o \times \begin{cases} 0 & \phi < -U < 0 \\ (1-\phi/U)(1-\delta) & -U < \phi < 0 \\ \beta(1-\phi/U)(1-\delta) & \phi \geq 0 \end{cases} \quad (3)$$

where δ is the energy-dependent secondary emission coefficient evaluated at an energy $E = eU + e\phi$. The velocity distribution of the secondary electrons can be described as Maxwellian with $kT_s \sim 3$ eV [*Whipple*, 1981]. For positively charged dust grains the fraction of the produced secondary electrons that can escape is $\beta = (1 + e\phi/kT_s)\exp(-e\phi/kT_s)$. The function $\delta(E)$ is often approximated as [*Sternglass*, 1954]

$$\delta(E) = 7.4\delta_M(E/E_M)\exp\left(-2(E/E_M)^{1/2}\right) \quad (4)$$

where the maximum yield δ_M and the optimum energy E_M (for which $\delta = \delta_M$) are material parameters. The Sternglass formula is strictly valid only for normal incidence onto plane surfaces. It is also a good approximation for isotropic incidence onto a spherical grain if the penetration depth of the primary electrons (about 100 Å for a 100 eV electron in glass) is much less than the grain radius [*Chow et al.*, 1993], which is the case in our experiment. However, the effective secondary yield for isotropic incidence is $\delta_{eff} \simeq 2\delta$ [*Draine and Salpeter*, 1979].

For a given fast electron energy (eU), the net current becomes zero as grains reach charge equilibrium,

$$\frac{dQ}{dt} = \frac{r_g d\phi}{dt} = J_f(eU, \phi, \delta_M, E_M) + J_e(eU, \phi) + J_i(eU, \phi) = 0, \quad (5)$$

the potential $\phi = Q/r_g$, where r_g is the radius of a dust grain.

Materials with a high enough secondary yield can exhibit multiple roots in (5) for a limited range of electron impact energies [*Whipple*, 1981; *Meyer-Vernet*, 1982; *Horányi et al.*, 1995]. An example of a multiple-roots case is shown in (Figure 3) for eU =60 eV, $\delta_M^{eff} = 3.2$ and $E_M = 400$ eV, using the plasma parameters in our apparatus.

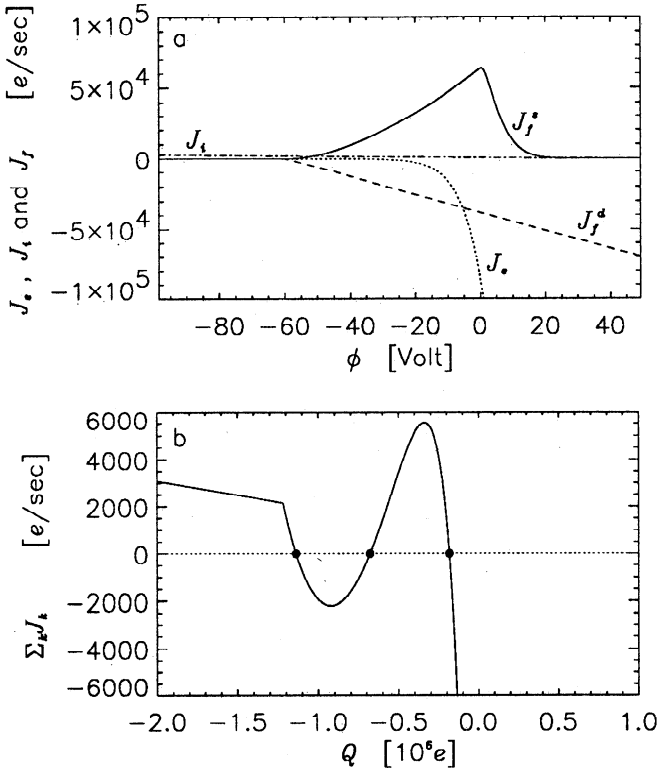

Figure 3. (a) Electron (J_e) and ion (J_i) thermal currents, and the fast electron current ($J_f = J_f^d + J_f^s$), with its direct and secondary contribution as functions of a grain's surface potential for the case of a grain with radius $r_g = 29$ μm, eU=60 eV, $\delta_M^{eff} = 3.2$, and $E_M = 400$. (b) Net current as a function of the grain's charge. Dots indicate equilibrium, where $dQ/dt = \sum_k J_k = 0$. The middle solution is unstable, i.e., a positive (negative) charge fluctuation generates a positive (negative) current driving the charge toward one of the two stable roots. In general, the "S" shaped part of this curve remains entirely above or below zero, and only one solution exists.

3. Experimental Results

Measurements were made using simulated lunar regolith materials MLS-1 and JSC-1 [*Weiblen et al.*, 1990; *McKay et al.*, 1994] and lunar soil samples returned by the Apollo 17 mission in 1972 from the southeastern rim of Mare Serenitatis [*Berg et al.*, 1973]. We sieved these materials to select particles with radii 29 ± 3 μm, the narrowest size distribution we could arrange for. Grains in this size range have sufficiently large signals in the Faraday cup. Our samples were stored in a vacuum dessicator to remove moisture. All our experimental results are shown in (Figure 4). At each beam energy eU, 50 charge measurements were made. In regions where the distribution of the 50 measured charges indicated a bimodal distribution due to the presence of two stable charge equilibria, we have split the data points into two groups and treated them independently.

The experimental data points for beam energies below $\simeq$50 eV show an approximately linear trend, since in the absence of significant secondary electron production, grains will charge to potentials set by the energy of the fast electrons alone. For higher beam energies, secondary electron production becomes significant, and it breaks the linear trend.

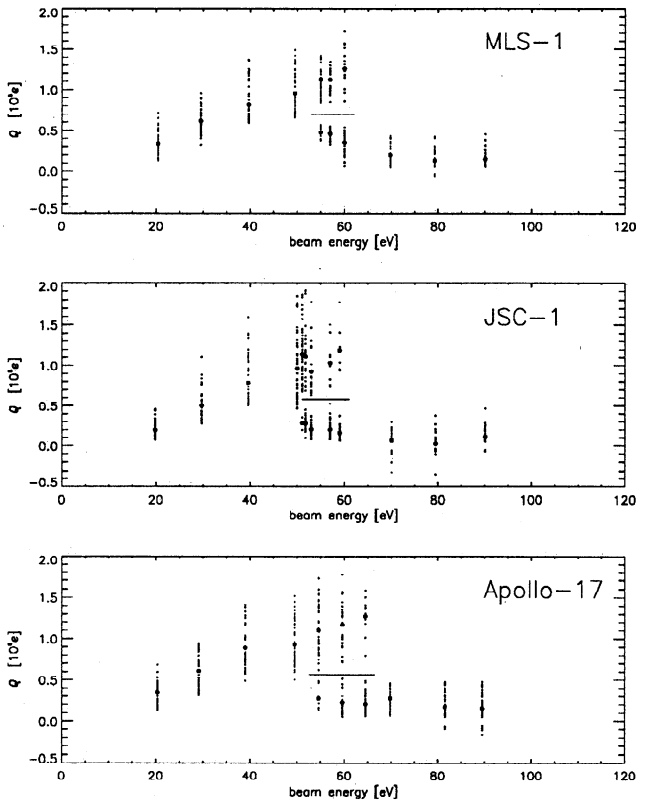

Figure 4. Measured charges (small dots) as function of the beam electron energy. The large dots represent the average of the measured charges, and the horizontal line separates the regions where the distribution of the measurements indicates multiple charge states.

We have used (5) and our plasma parameters (Figure 2) to calculate the expected charges for each beam electron energy setting as function of the two free material parameters δ_M^{eff} and E_M, in order to minimize

$$\chi^2(\delta_M^{eff}, E_M) = \frac{1}{\langle\sigma^2\rangle} \sum_{i=1}^{N} \left(Q_i^M - Q_i^C(\delta_M^{eff}, E_M)\right)^2, \quad (6)$$

where $\langle\sigma^2\rangle$ is the average standard variation for a given sample material, N is the number of data points, Q_i^M is the average of the measured charges, and Q_i^C is the calculated charge for the same fast electron energy.

For each material we made a "grid" search first by varying E_M in the range of $300 \leq E_M \leq 700$ eV in steps of $\Delta E_M = 10eV$ and δ_M^{eff} in the range of $1 \leq \delta_M^{eff} \leq 5$ in steps of $\Delta\delta_M^{eff} = 0.1$. These are larger than the expected ranges for lunar dust [*Willis et al.*, 1973]. We used the resulting map to identify the regions where $\chi^2(\delta_M^{eff}, E_M)$ were minimized. To avoid possible aliasing, next we generated 10,000 random (δ_M^{eff}, E_M) pairs to uniformly cover the region where the minimum of $\chi^2(\delta_M^{eff}, E_M)$ was expected. For each material the minimum of χ^2 identified a narrow region in the (δ_M^{eff}, E_M) space that could be well-fit with a straight line (Figure 5). The reason for finding a set of solutions and not just one (δ_M^{eff}, E_M) pair is that for bombarding electron energies below 100 eV the resulting secondary yield, δ, shows negligible difference along the minimum χ^2 lines (Figure 6).

The results of our linear regression fits to the minimum χ^2 points (for $300 \leq E_M \leq 700$ eV) are [*Press et al.*, 1992]

$$\text{MLS}-1: \quad \delta_M^{eff} = (1 \pm 0.1) + 0.52 \times 10^{-2} E_M$$
$$\text{JSC}-1: \quad \delta_M^{eff} = (1 \pm 0.1) + 0.59 \times 10^{-2} E_M$$
$$\text{Apollo 17}: \quad \delta_M^{eff} = (1 \pm 0.1) + 0.54 \times 10^{-2} E_M$$

To compare these results to our earlier and simpler analysis [*Horányi et al.*, 1995], we also list δ_M^{eff} for the case, where we assume $E_M = 400$ eV for all the sample materials

$$\text{MLS}-1: \quad \delta_M^{eff} = 3.1 \pm 0.1$$
$$\text{JSC}-1: \quad \delta_M^{eff} = 3.4 \pm 0.1$$
$$\text{Apollo 17}: \quad \delta_M^{eff} = 3.2 \pm 0.1$$

These are all similar to the measured values of the Apollo 14 and 15 samples of $\delta_M = 1.5 \pm 0.1$ (i.e., for

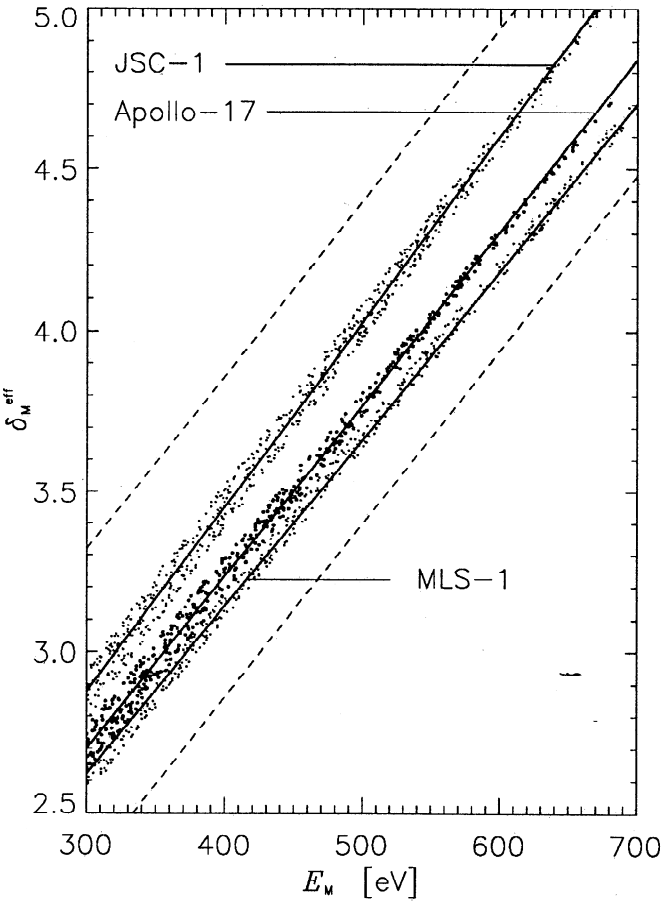

Figure 5. Set of E_M, δ_M^{eff} pairs that minimize χ^2 (6) and the linear fits to these points. Dashed lines show the region where we randomly selected 10,000 E_M, δ_M^{eff} pairs to evaluate χ^2. For all of the points shown, $\chi^2_{min} < \chi^2 < 1.2\chi^2_{min}$, where $\chi^2_{min} \simeq 60$ (11 degrees of freedom, dof), 130 (15 dof), and 50 (11 dof) for JSC-1, MLS-1, and Apollo 17 samples, respectively.

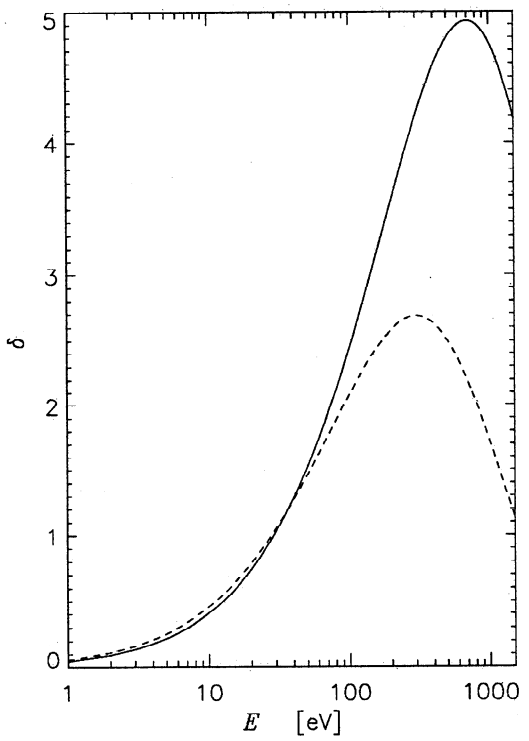

Figure 6. Secondary electron yield from (4) as function of the energy of the impacting electrons for the parameters $\delta_M = 2.7, E_M = 300$ (dashed line), and $\delta_M = 4.8, E_M = 700$ (solid line), the end points of the linear fit to our Apollo 17 data in Figure 5. For $E < 100$ eV the difference between these curves is negligible and our experiments cannot distinguish them.

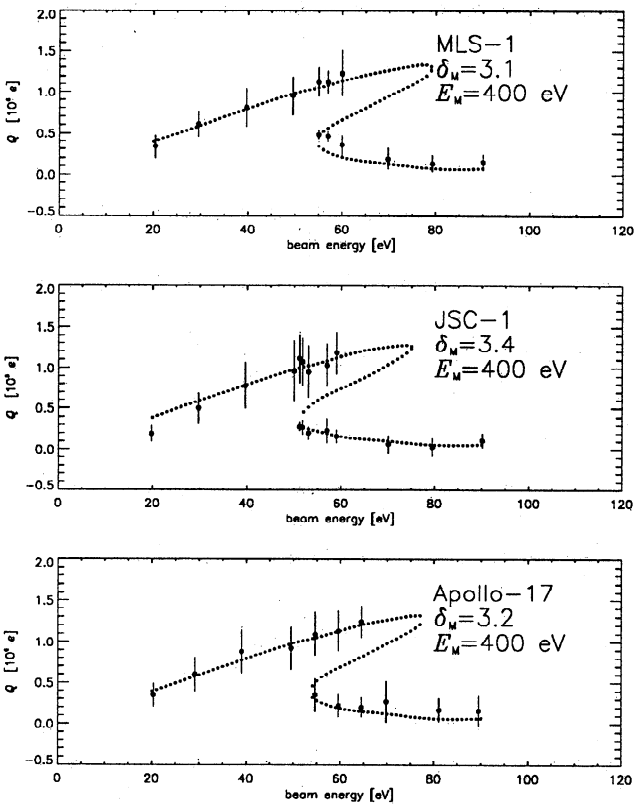

Figure 7. Average of the measured charges (dots) with error bars to show one standard deviation and our fits setting $E_M = 400$ and $\delta_M^{eff} = 3.1$ for MLS-1 (top), $\delta_M^{eff} = 3.4$ (middle), and $\delta_M^{eff} = 3.2$ for the Apollo 17 (bottom) soil sample.

isotropic incidence $\delta_M^{eff} = 3.0 \pm 0.2$) in the range of $300 E_M \leq E_M \leq 700$ eV [*Willis et al.*, 1973]. The fits to the measurements are shown in (Figure 7).

4. Summary and Conclusion

We measured the electrostatic charging of simulated lunar materials JSC-1 and MLS-1, and also a soil sample from the Moon collected during the Apollo 17 mission. The secondary electron production from these materials, in the energy range of $20 \leq E \leq 90$ eV of the bombarding electrons, are similar. The measured secondary electron yield for the Apollo 17 sample was intermediate between MLS-1 and JSC-1 simulants, closer to that of MLS-1. We have verified that multiple charge states could exist on the Moon as it traverses through the plasma tail of Earth, where it encounters an energetic plasma environment.

On the dayside of the Moon, photoelectron production becomes dominant. We are now modifying our plasma chamber to accommodate a solar UV simulant light source to examine charging due to photoelectron production.

Our long-term goal remains to develop a laboratory lunar surface model, where time dependent illumination and plasma bombardment will closely emulate the conditions on the surface of the Moon.

Acknowledgments. This project was funded by the Planetary Materials and Geochemistry Program of NASA (NAG-6138). We thank the Curation and Analysis Planning Team (CAPTEM) for supplying the Apollo 17 lunar soil sample and J.A. Nuth III and C.B. Pilcher for their support.

References

Berg, O. E., A lunar terminator configuration, *Earth Planet. Sci. Lett.*, *39*, 377–381, 1978.

Berg, O. E., F. F. Richardson, and H. Burton, Apollo 17 Preliminary Science Report, *NASA Spec. Publ. SP-330*, 16, 1973.

Chow, V.W., D.A. Mendis, and M. Rosenberg, The role of grain size and particle velocity distribution in secondary electron emission in space plasmas, *J. Geophys. Res.*, *98*, 19,065, 1993.

Criswell, D. R., Horizon glow and the motion of lunar dust, in *Photon and Particle Interaction in Space*, edited by R. J. L. Grard, pp. 545-556, D. Reidel, Norwell, Mass., 1973.

Criswell, D. R., and B. R. De, Intense localized charging in the lunar sunset terminator region: Supercharging at the progression of sunset, *J. Geophys. Res.*, *82*, 1005, 1977.

De, B. R., and D. R. Criswell, Intense localized charging in the lunar sunset terminator region: Development of potentials and fields, *J. Geophys. Res.*, *82*, 999, 1977.

Draine, B.T., and E.E. Salpeter, On the physics of dust grains in hot gas, *Astrophys. J.*, *231*, 77-94, 1979.

Goertz, C. K., Dusty plasmas in the solar system, *Rev. Geophys.*, *27*, 271, 1989.

Gold, T., and G.J. Williams, Electrostatic transportation of dust on the moon, in *Photon and Particle Interactions with Surfaces in Space*, edited by R. J. L. Grard, pp. 557, D. Reidel, Norwell, Mass., 1973.

Hershkowitz, N., How Langmuir probes work, in *Plasma Diagnostics*, edited by O. Auciello and D. Flamm, pp. 113, Academic, San Diego, Calif., 1989.

Horányi, M., S. Robertson, and B. Walch, Electrostatic charging properties of simulated lunar dust, *Geophys. Res. Lett., 22*, 2079, 1995.

McDaniel, E.W., *Collision Phenomena in Ionized Gases*, John Wiley, New York, 1964.

McKay, D. S., J. L. Carter, W. W. Boles, C. C. Allen, and J. H. Allton, JSC-1: A new lunar soil simulant, in *Engineering, Construction, and Operations in Space IV*, vol. 2, Am. Soc. of Civ. Eng., Reston, Va., 1994.

Meyer-Vernet, N., "Flip-flop" of electric potential of dust grains in space, *Astron. Astrophys., 105*, 98-106, 1982.

Press, W.H., S.A. Teukolsky, W.T. Vetterling and B.P. Flannery, *Numerical Recipes*, Cambridge Univ. Press, New York, 1992.

Propenko, S.M.L., and J.G. Laframboise, High-voltage differential charging of geostationary spacecraft, *J. Geophys. Res., 85*, 4125-4131, 1980.

Rennilson, J. J., and D. R. Criswell, Surveyor observations of lunar horizon glow, *Moon, 10*, 121, 1973.

Singer, S. F., and E. H. Walker, Electrostatic dust transport on the lunar surface, *Icarus, 1*, 112, 1962.

Sternglass, E.J., Backscattering of kilovolt electrons from solids, *Phys. Rev., 95*, 345-58, 1954.

Walch, B., M. Horanyi, and S. Robertson, Charging of dust grains in plasma with energetic electrons, *Phys. Rev. Lett., 75*, 838, 1995.

Weiblen, P. W., M. J. Murawa, and K. J. Reid, Preparation of simulants for lunar surface materials, in *Engineering, Construction, and Operations in Space II*, vol. 1, p. 98, Am. Soc. of Civ. Eng., Reston, Va., 1990.

Whipple, E.C., Potential of surfaces in space, *Rep. Prog. Phys., 44*, 1197-1250, 1981.

Willis, R. F., M. Anderegg, B. Feuerbacher, and B. Fitton, Photoemission and secondary electron emission from lunar surface materials, in *Photon and Particle Interactions with Surfaces in Space*, edited by R. J. L. Grard, pp. 389, D. Reidel, Norwell, Mass., 1973.

Zook, H.A., and J.E. McCoy, Large-scale lunar horizon glow and a high altitude lunar dust exosphere, *Geophys. Res. Lett., 18*, 2117-2120, 1991.

D. Alexander and S. Robertson, Physics Department, University of Colorado, Boulder CO 80309-0391. (e-mail: alexanda @plasma. colorado.edu; robertso @stripe.colorado.edu)

M. Horányi, Laboratory for Atmospheric and Space Physics, University of Colorado, Boulder, CO 80309-0392. (e-mail: horanyi@styx.colorado.edu)

B. Walch, Department of Physics, University of Northern Colorado, Greeley, CO 80639. (e-mail: rwalch @bentley.unco.edu)

(Received November 24, 1997; revised February 4, 1998; accepted February 10, 1998.)